Lifetime of the 981-keV State in Li^8†

M. J. Throop*
University of Iowa, Iowa City, Iowa 52240
and
D. H. Youngblood
Texas A & M University, College Station, Texas 77843
and
G. C. Morrison
Argonne National Laboratory, Argonne, Illinois 60439
(Received 17 November 1970)

The lifetime of the 981-keV state in Li^8 produced in the $D(Li^7,p)Li^{8*}$ reaction was measured by the two-backing variant of the Doppler-shift attenuation method. The resulting mean life was $\tau_m = 10.1 \pm 4.5$ fsec. This result is in agreement with the shell-model prediction of Cohen and Kurath, and also with that of Barker. The large error limits preclude a detailed test of either prediction.

I. INTRODUCTION

Radiative lifetimes of nuclear states may in many cases be compared with specific theoretical predictions for these levels and can provide a sensitive test for the models on which such predictions are based. We report here a measurement of the lifetime of the Li^8 first excited state at 981 keV by means of the attenuated-Doppler-shift technique and a comparison of the result with predictions of a shell-model calculation for the $1p$ shell.[1] An upper limit of 35 fsec for this lifetime has been previously reported.[2]

II. EXPERIMENTAL PROCEDURE

A. Doppler-Shift Measurements

The 981-keV ($J^\pi = 1^+$) first excited state in Li^8 was populated with the $D(Li^7,p)Li^{8*}$ reaction [$Q = -1.173$ MeV, threshold at $E(Li^7) = 5.278$ MeV] at a bombarding energy of 7.40 MeV. Typical beam currents of 40–80 nA of doubly-charged Li^7 ions were obtained from the University of Iowa 5.5-MeV Van de Graaff with the aid of an internal carbon stripper assembly.[3] The Li^7 bombarding energy was chosen to reduce the spread in angle and velocity of the recoiling Li^{8*}, yet still give an adequate yield; the recoiling nuclei were confined to a cone with a half angle of 6°.

The γ rays were recorded in a 20-cm^3 coaxial Ge(Li) detector having a resolution width of 5.5 keV for 1.33-MeV γ rays. Spectra were recorded in 2048 channels spanning the energy range from 500 to 1300 keV. The radiation from the target was accumulated simultaneously with reference lines[4] from Mn^{54} (834.81 keV) and Zn^{65} (1115.40 keV) sources. Zero and gain-shift corrections were applied by a pair of digital stabilizers set on the reference lines. A 1-in.-thick graphite absorber was placed in front of the detector in order to suppress background from the β decay of Li^8.

The 981-keV γ-ray transition observed at 0° to the beam axis was expected to be shifted upward in energy to 1017 keV (unattenuated shift). Since the lifetime was known to be much shorter than the slowing-down times typically obtainable with solid materials, the attenuation was not expected to exceed a few percent of the total shift. Thus the method used by Blaugrund *et al.*[5] was employed. It involves an accurate measurement at 0° of the difference between the energy of the Doppler-shifted γ ray for a gas target (full shift – no significant slowing down of the recoiling nucleus before decay) and the energy of the Doppler-shifted γ ray for a solid target (attenuated shift – target material chosen to maximize the slowing-down time).

The attenuated shift obtained with a deuterated Zr target[6] (113-$\mu g/cm^2$ Zr on a 10-mil Pt backing) was compared with the full shift obtained with a D_2 gas target at pressures of 12–18 Torr. The experimental arrangement for the gas target was identical to that for the solid target except for pressurization with D_2 gas and substitution of a beam stop consisting of an ~100-$\mu g/cm^2$ layer of undeuterated Zr on a 10-mil Pt backing (Fig. 1). The energy lost by the incoming 8.0-MeV Li^7 beam as it traversed the 0.57-mg/cm^2 Ni entrance window used in both target assemblies was calculated to be ~600 keV.

Two separate sets of measurements were made,

in each of which runs with gas and solid targets were alternated in order to avoid the effects of systematic drifts. Typical spectra are shown in Fig. 2. The Li^8 γ-ray energy measured at 90° was 981 ± 1 keV. The value obtained at 0° with the gas target (1017.0 ± 0.5 keV) is in agreement with that calculated from kinematics. In order to identify contaminant peaks, spectra were obtained for C and O targets at a Li^7 energy of 7.4 MeV. In Fig. 2, the peaks from the Li^7+C reaction are those at 871 keV (from the 0.871 → 0.0-MeV transition in O^{17}) and at 960 keV (the double-escape peak from the 1.98 → 0.0-MeV transition in O^{18}). Peaks from the Li^7+O reaction are those at 891 keV (the 0.891 → 0.0-MeV transition in Na^{22}) and 1133 keV (the 2.86 → 1.75-MeV transition in Ne^{21}). The peak at 937 keV (the 0.937 → 0.0-MeV transition in F^{18}) is from both C and O reactions. The remaining contaminant peaks, those at 842 keV and 1.04 MeV, are associated with the $Al^{27}(n, n')$ reactions, respectively.

In order to discover contaminant peaks in the energy region of the Doppler-broadened Li^8 peak, the γ-ray spectra from the C and O targets and from the D_2 gas target were measured with the incident Li^7 beam energy below the threshold for production of the 981-keV state in Li^8. The only peak found was a 1020.2 ± 1.0-keV peak in the spectrum from the C target; it was identified as the 2.10 → 1.08-MeV transition in F^{18} (E_γ = 1021.3 ± 1.2 keV, 33% branch[7]). The accompanying 2.10 → 0.94-MeV transition in F^{18} was also observed with about equal intensity, as expected. A third set of runs with a 25-cm^3-coaxial detector of improved resolution and a freshly prepared ZrD target was rendered unusable by the discovery of an omnipresent strong 1014.8-keV peak, in addition to the one at 1021.3 keV. The 1014.8-keV peak could be attributed only to a neutron-induced reaction in the detector housing material.

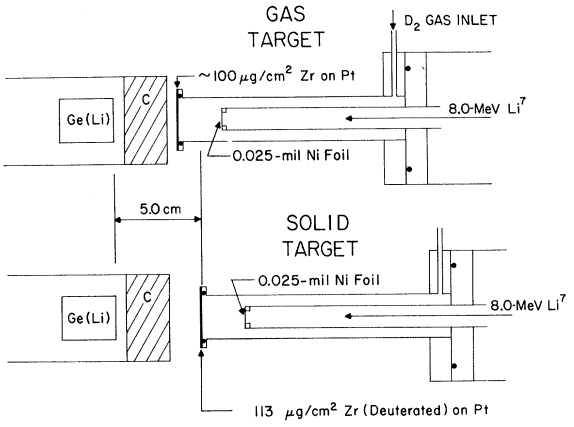

FIG. 1. Experimental arrangements used in measurements with gas and solid targets. To keep the detector-target distance the same for the gas- and the solid-target assemblies, the Ge(Li) detector was moved along the beam axis.

The relative intensities of the 1020.2-keV peak from F^{18} and the prominent 871-keV peak from O^{17} were determined from the spectrum obtained with the C target. Hence a measurement of the O^{17} peak intensity in the spectra from gas and solid targets could be used to determine the intensity of the F^{18} peak, which was not resolved from the Li^8 Doppler-shifted peak. The F^{18} transition contributed about 8% of the observed Li^8 peak in the spectra from the solid target and 0.3–3% in the spectra from the gas target, the particular value depending on the gas pressure and the level of carbon contamination.

The background in the region of the reference lines was checked by accumulating spectra for the gas and solid targets with the Mn^{54} and Zn^{65} sources absent. No peaks were seen in the spectral region normally occupied by the Zn^{65} peak. An 834.8-keV peak due to the $Ge^{72}(n, n')$ reaction was observed in the region normally occupied by the Mn^{54} peak. By suitable positioning of the source, the Mn^{54} reference peak was made sufficiently intense that the $Ge^{72}(n, n')$ had only an insignificant influence on the centroid of the reference peak.

B. Target Composition

The deuterated Zr targets were found to contain significant amounts of oxygen. These oxygen contents were determined from that of a vapor target consisting of D_2O at a known pressure by comparing their respective yields of the 1.28 → 0-MeV transition in Ne^{22} – a prominent peak resulting from the $O^{16}(Li^7, p)Ne^{22}$ reaction in oxygen targets. The deuterium contents of the solid targets were similarly determined by comparing the yields of the Li^8 peak for the solid gas targets after correction for underlying contaminant contributions. The solid target used in the two sets of measurements contained 113 $\mu g/cm^2$ of Zr as determined by weighing[6] before deuteration. On the basis of this weight of Zr, the formula for the target materials could be written as $ZrO_{1.10}D_{0.69}$; this corresponds to a total thickness of 140 $\mu g/cm^2$.

In view of the significant amount of oxygen discovered in the target, it seemed worthwhile to further check the composition and uniformity of the target material and the possible presence of other target contaminants. To this end, the spectrum of 5.0-MeV α particles backscattered from the target layer and its Pt backing was compared with the backscattered spectrum for a Pt backing alone. Both spectra, measured at 150°, are

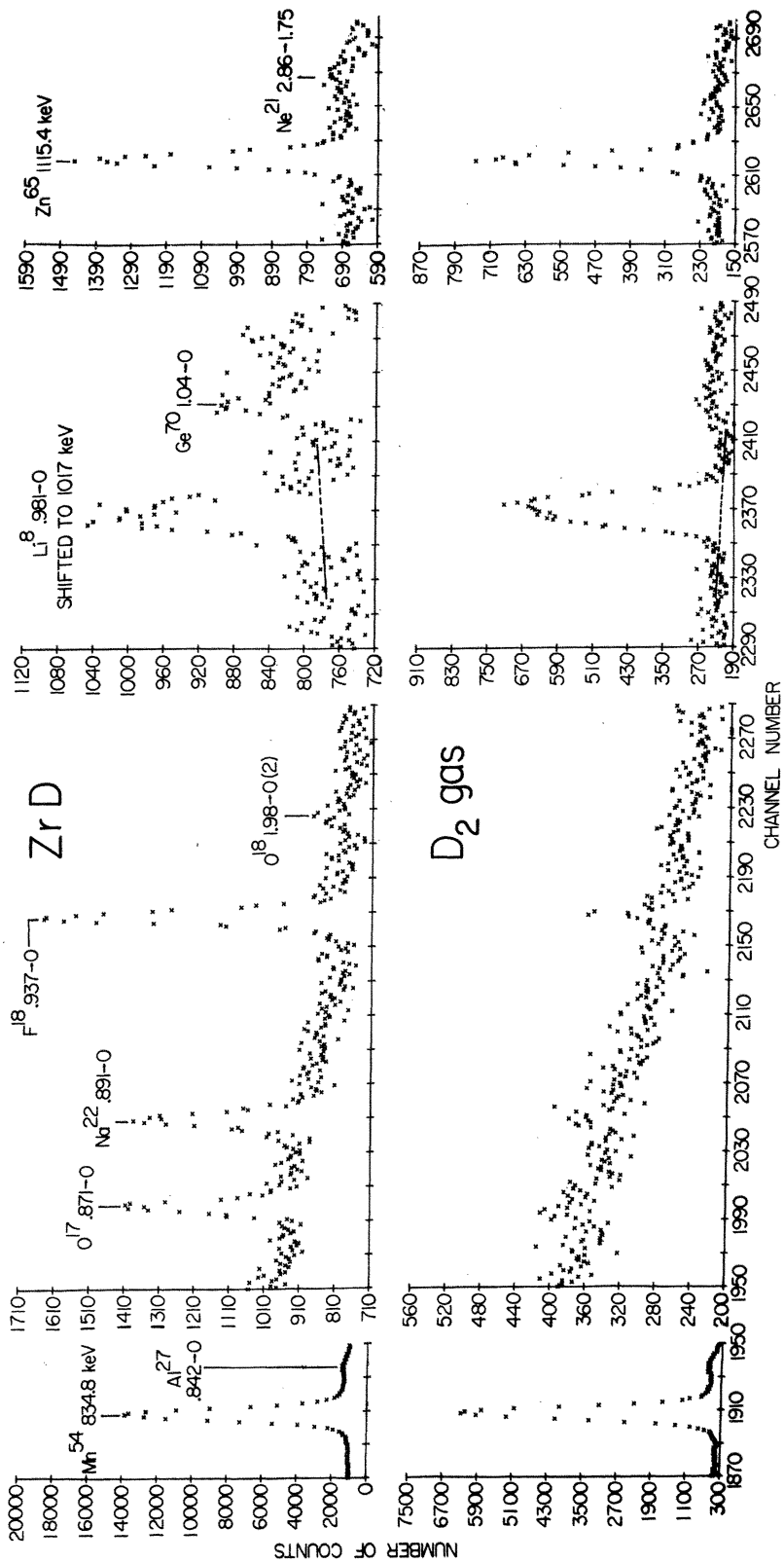

FIG. 2. Portions of the γ-ray spectra obtained for deuterated Zr and D_2 gas targets at 0°. Note the change in the ordinate scale for different portions of the spectra. The energy dispersion is 0.395 keV/channel. The Mn^{54} and Zn^{65} reference peaks are identified by their γ-ray energies; all other peaks are identified by the final nucleus and the transition therein. Transitions in Ge and Al resulted from the (n,n') reaction with detector materials. The dashed lines indicate the background chosen in the centroid analysis of the Li^8 peak.

shown in Fig. 3. The initial steep rise at the highest energies in each curve represents the onset of backscattering at the front of the platinum. Hence the difference ΔE_{TGT} between the positions of these rises represents the energy lost by the α particles as they are slowed down in penetrating and returning through the target layer – i.e., in twice traversing the layer of Zr and contaminants.

The peak due to scattering in the thin Zr layer is located at lower energies (on the flat portion of the Pt spectrum) since more energy is lost in scattering from a Zr nucleus than from the heavier Pt. The width of the peak corresponds to the difference between the energy losses of α particles scattered from Zr nuclei at the front and back of the target layer, so ΔE_{Zr} (corrected for detector resolution) represents the slowing-down loss as the α particles penetrate and return through the Zr layer. It was found that ΔE_{Zr} is about 16 keV less than ΔE_{TGT}, a difference attributable to the slowing-down loss in a 10-μg/cm^2 carbon layer on the Zr. The existence of the C layer was confirmed by the shift in position of the leading edge of the Zr peak (Fig. 3) compared to other Zr-on-Pt targets and by a comparison between the γ rays produced in the target and those from a C target of known thickness. In addition, when the energy loss for a target of this composition is calculated from α-particle stopping-power tables,[8] the result agrees with the observed loss only if the carbon layer on the front of the target is taken into account.

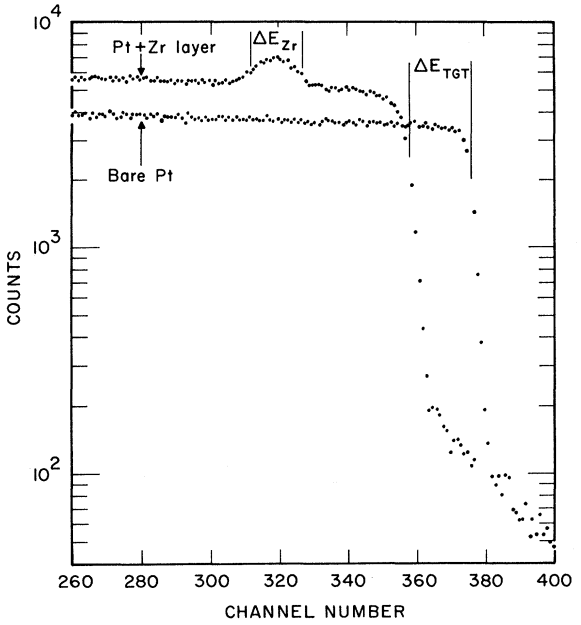

FIG. 3. Spectrum of 5.0-MeV α particles backscattered at 150° from bare Pt and from the 140-μg/cm^2 Zr target with Pt backing. ΔE_{TGT} represents the α-energy loss in the Zr layer and in the contaminant layers present on the Pt backing; ΔE_{Zr} represents the α-energy loss for the layer in which Zr atoms are distributed. Note that ΔE_{Zr} is less than ΔE_{TGT}; the difference is the slowing-down loss in a C layer on the Zr.

The width and shape of the Zr peak was consistent with a uniform distribution of Zr and O throughout the target layer. No conclusions could be drawn about the distribution of deuterium which (fortunately) contributed very little to the stopping power of the target layer.

Possible uncertainties in the composition of the gas target were associated with properties of its beam stop, which was a Pt backed layer of undeuterated Zr in order to reproduce exactly the background conditions resulting from use of the solid target. When exposed to the gas, the stop collected a small amount of deuterium, but this produced a negligible shift in the energy of the Li^8 peak.

III. DATA ANALYSIS

A. Measured Differences

The background was determined by least-squares-fitting a polynomial to selected portions of the background spectrum on each side of the peak of interest. The background underneath the peak was assumed to be a smooth continuation of that on either side. The regions chosen for background fits to the Mn^{54}, Li^8, and Zn^{65} peaks were kept fixed for all the gas- and solid-target runs on each set of measurements. The centroids of the Li^8 peaks and the associated absolute peak energies were found to be somewhat dependent on the choice of the region for the background fit. How-

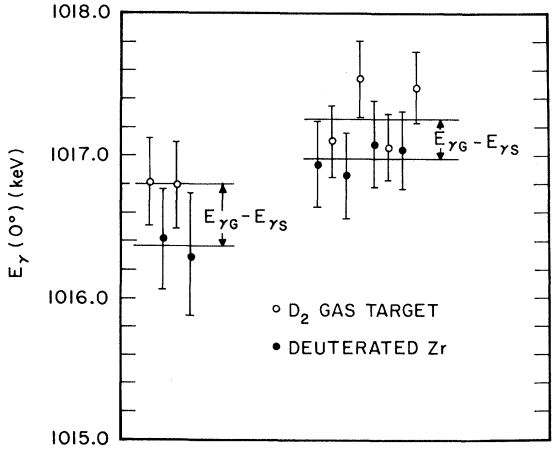

FIG. 4. Differences between the γ-ray energies measured at 0° for gas and solid targets. The weighted average energy difference $(E_{\gamma G} - E_{\gamma S})$ is shown for each set.

ever, the energy *difference* between gas and solid targets was found to be independent of the region chosen for the background fit, so long as the fit was over the same spectral region for both gas and solid target. Typical background fits are shown in Fig. 2.

The centroid energies of the Li^8 peak (Fig. 4) were determined by linear interpolation from the energies of the Mn^{54} and Zn^{65} reference lines. Differences between the absolute Li^8 energies in the two sets of measurements are due to differing experimental conditions. The Li^8 γ-ray energy for the gas target was consistently higher than that for the corresponding solid target. The error-weighted averages of the differences $(E_{\gamma G} - E_{\gamma S})$ between the energies for the gas and solid targets in the two sets of measurements are listed in Table I. Several corrections to the observed gas-solid differences were necessary and are discussed below.

TABLE I. Averaged differences between the Li^8 γ-ray energies for gas and solid targets in two sets of measurements. Also listed for each set are corrections arising from differences between the gas and solid targets – differences in target thickness, in the geometric distribution of target material, and in the amounts of contaminant.

	Set I (eV)	Set II (eV)
$(E_{\gamma G} - E_{\gamma S})$	440 ± 330	290 ± 190
Target-thickness correction	−200 ± 95	−170 ± 100
Geometric correction	+50 ± 20	+50 ± 20
Contaminant correction	+300 ± 140	+190 ± 110
$(E_{\gamma\infty} - E_{\gamma\alpha})$	590 ± 370	360 ± 240
Weighted average	430 ± 200	

B. Target-Thickness Correction

The mean Li^7 energy at which the $D(Li^7, p)Li^{8*}$ reaction occurred was less for the relatively thicker solid target than for the gas target. The difference between the effective energies of the reactions in the gas and solid targets results in a difference between the recoil energies and a significant correction to the observed energy difference between the energies of the Doppler-shifted γ rays.

A mean Li^7 energy loss for each target was calculated from the stopping power and thickness of the individual target constituents. The stopping power of D_2 gas for Li was determined by extrapolation from lower-energy data for Li stopping in H_2.[9] Data for Li stopping in Zr, O, and Pt were not available. (A knowledge of Li stopping in Pt was not necessary in computing the mean Li^7 energy but was necessary in calculating the Li^8 lifetime from the observed difference in Doppler shifts.) Stopping powers were calculated in two ways – by extrapolation of data for Li stopping in Ag, N_2 and C, and Au, respectively,[9] and by multiplying data[10] for proton stopping at an equivalent velocity in Zr, O, and Pt by a velocity-dependent average charge for the Li ion.[11] The values obtained by the two methods agreed well within the estimated error of ±15%. Calculated dE/dx values for the ZrOD target and Pt backing are shown as a function of velocity in Fig. 5.

The mean energy loss in each target determines the mean Li^7 energy for the reaction. The deuterium was assumed to be uniformly distributed throughout the target layer. Error limits on the mean energy correspond to the assumption that the deuterium was uniformly concentrated in either the front or back half of the target layer. (The calculated stopping power of the target is not affected by the deuterium distribution.) Variation in the $D(Li^7, p)Li^{8*}$ cross section is less than ±6% over the range of Li^7 energies in the solid target,[12] so any effect on the mean energy could be neglected.

The target-thickness corrections to the observed

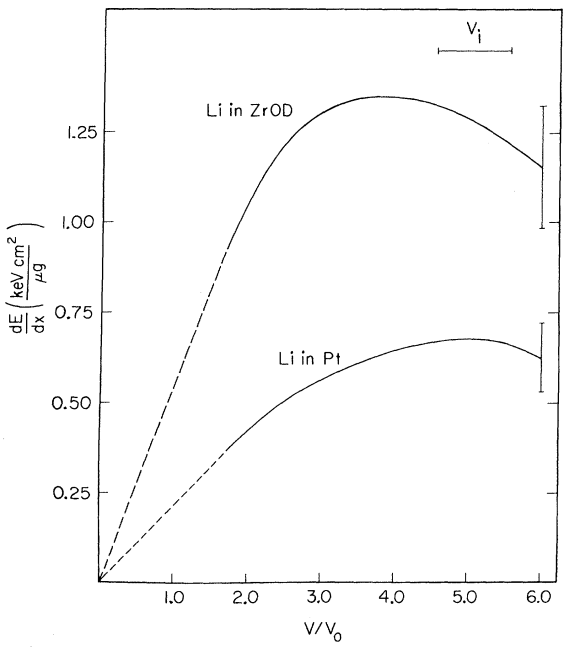

FIG. 5. Calculated stopping power vs velocity (v/v_0, where $v_0 = c/137$) for Li stopping in the ZrOD target layer and the Pt backing. Vertical lines at $v/v_0 = 6$ indicate uncertainty in the stopping power; the horizontal line labeled v_i indicates the kinematic spread in initial Li^{8*} velocities. An insignificant fraction of the Li^{8*} decays occurred in the velocity region of the dashed portion of the curves, which are a simple linear extrapolation from stopping power at higher velocities.

differences in the energies of Li^8 γ rays were calculated for the different effective energies and are listed in Table I. The correction includes a 40-eV contribution due to the ~10-$\mu g/cm^2$ carbon layer. The quoted error combines those arising from the uncertainty in the knowledge of the stopping power and of the deuterium distribution.

C. Geometric Correction

The distance from the center of the target to the detector was 5.0 cm for all measurements. Hence the first-order finite-solid-angle attenuation of the Doppler shift was the same for the gas and solid targets. The second-order effect due to the finite length of the gas target (2.65 cm) was calculated by integration over the active volume of the detector. The resulting geometric corrections are listed in Table I.

The position of the detector with respect to the center of the target could be reset to an estimated ±1 mm. The resulting ±40-eV uncertainty in the Doppler-shifted energy was negligible compared to other sources of error. A further ±40-eV maximum uncertainty due to imperfect coincidence between the axis of the detector and the beam axis was also neglected.

D. Correction for Contaminant Peak

The contaminant peak at 1020.2 keV could not be resolved from the Doppler-broadened Li^8 peak. The centroid of the observed peak was related to the centroid of the Li^8 and the contaminant peak by

$$N_T C_T = N_L C_L + N_A C_A ,$$

with

$$N_T = N_L + N_A ,$$

where N is the number of counts in a peak, C is the centroid energy of the peak, and the subscripts T, L, and A refer to the total observed peak, the Li^8 peak, and the contaminant peak, respectively. The correction $(C_T - C_L)$ was determined for the gas and solid targets in each set of runs.

The resulting contaminant corrections (those due to the difference between the contaminant in the gas and solid targets) are listed in Table I. Errors in these corrections are due about equally to uncertainty in the energy and uncertainty in the intensity of the contaminant peak.

E. Variation Over the Entrance Window

A significant difference could be obtained between two measurements if the beam were focused on different portions of the Ni window, since a 20% variation in window thickness[13] was equivalent to a ±120-keV variation in beam energy or to a ±300-eV variation in the Li^8 γ-ray energy. This variation was expected to have a random character, however, since the beam was refocused for each measurement. The numerous measurements in each set were made alternately with the gas and solid targets, and each set employed a different Ni window. Thus the errors in the observed difference $(E_{\gamma G} - E_{\gamma S})$ listed in Table I, which were determined from the internal scatter of the data (Fig. 4), include the error due to any nonuniformity in window thickness.

F. Lifetime Determination

For each set of measurements the observed energy difference $E_{\gamma G} - E_{\gamma S}$ and the corrections to this difference were combined (Table I) to obtain a value of the corrected difference which, in the notation of Ref. 5, is $E_{\gamma\infty} - E_{\gamma\alpha}$. The average of the two corrected differences, weighted by the absolute errors in the numbers, is

$$E_{\gamma\infty} - E_{\gamma\alpha} = 430 \pm 200 \text{ eV},$$

and hence,

$$(E_{\gamma\infty} - E_{\gamma\alpha})/\Delta E_{\gamma\infty} = 0.0122 \pm 0.0057 ,$$

where $\Delta E_{\gamma\infty}$ is the difference in energy between the fully shifted and the unshifted γ ray. The value $\Delta E_{\gamma\infty} = 35.3 \pm 1.0$ keV was calculated from kinematics and included a 2% reduction due to the finite solid angle of the γ-ray detector. The error is based on an estimate of the uncertainty in the c.m. angular distribution of Li^{8*} nuclei. The calculated value of $\Delta E_{\gamma\infty}$ is in good agreement with the measured shift of 36 ± 1 keV between the measurements at 0 and 90°.

The shift difference as a function of lifetime was calculated by use of a computer code capable of evaluating the Doppler-shift-attenuation inte-

TABLE II. Comparison of the experimental $M1$ transition strengths for the 0.981-MeV state in Li^8 and the 0.780-MeV analog state in B^8 with theoretical calculations. (See Refs. 1 and 15.)

State	τ_m (fsec)	Transition strength $B(M1)$ Exp.	(6-16)-2B	(8-16)-POT
Li^8 (0.981)	10.1±4.5	6.0±2.7	4.6	0.5
B^8 (0.870)	13[a]	9	3.6	•••

[a] P. Paul, S. S. Hanna, T. R. Fisher, F. Riess, and J. B. Thomas, in *Symposium on Recent Progress in Nuclear Physics with Tandems, Heidelberg, Germany, 18–21 July 1966,* edited by W. Hering (Max Planck Institute for Nuclear Physics, Heidelberg, Germany, 1966), p. 71.

gral for lifetimes as short as 1 fsec. The shift difference to be compared with that determined experimentally was an average over the differences calculated for a number of Li^{8*} starting points in the target layer and included the possibility of slowing down in the Pt backing. An appropriate average was also taken over the spread of Li^{8*} angles and velocities on the assumption that the Li^{8*} velocities were distributed isotropically in the c.m. system. The stopping-power curves (Fig. 5) were used in the calculation. The effects of nuclear stopping and scattering were included in the calculation, although these did not affect the lifetime result by more than a few percent owing to the high initial velocity of the recoiling Li^{8*}. The density of the target layer was taken as $\rho = 6.0 \pm 0.5$ g/cm^3, an interpolation between the densities of Zr ($\rho = 6.4$ g/cm^3) and ZrO_2 ($\rho = 5.5$ g/cm^3).

The resulting mean lifetime for the 981-keV state in Li^8 is

$$\tau_m = 10.1 \pm 4.5 \text{ fsec}.$$

The error includes the effects of the uncertainty in the density of the target layer and a ±15% uncertainty in the data on the stopping powers of the target layer and backing. This result supersedes the earlier one[14] which was based on a preliminary analysis of our results.

IV. DISCUSSION

In Table II this result for the lifetime of the 981-keV transition in Li^8 and the lifetime of the 780-keV analog transition in B^8 are compared with the shell-model predictions of Cohen and Kurath,[1,15] who obtained effective interactions in the $1p$ shell by fitting experimental level energies. Experimental values of the transition strengths $B(M1)$ were obtained from the experimental lifetimes by use of the relation $\hbar/\tau_m = \Gamma_{M1} = 11.56 \times 10^{-3} E_\gamma^3 B(M1)$, where Γ_{M1} is in eV and E_γ is in MeV.

The predicted transition strengths are sensitive to the interaction chosen; the strength based on the (8-16)-POT interaction[1] is well outside the experimental limits for Li^8, while that based on the (6-16)-2B interaction[1] gives good agreement. Although generally lower than the experimental values, the theoretical results for the Li^8 and B^8 states are sensitive to mixing of the two lowest $J = 1^+$, $T = 1$ states, since these have large $M1$ matrix elements to the ground state. If these are mixed in phase, the theoretical values for the (6-16)-2B interaction become 8.5 for Li^8 and 8.1 for B^8. Such a mixing procedure has been necessary to obtain agreement with experimental results for B^{10} transitions.[16]

The present Li^8 result also agrees within the experimental limits with the theoretical value $B(M1) = 4.47$ obtained by Barker,[17] who used shell-model wave functions that correctly reproduced the speed of the analog transition in Be^8.

The rather large error limits on the present result preclude a detailed test of either theoretical calculation. In the comparison with the predictions of Cohen and Kurath, for example, only the choice of interaction is tested; the mixing required to bring the theoretical transition strengths into agreement with experiment cannot be usefully estimated.

ACKNOWLEDGMENTS

The authors wish to thank Professor R. R. Carlson for a number of useful suggestions made in discussions throughout the course of this work, and in particular for suggesting the α-backscattering method used in determining the composition of the target layer. G. W. Hartnell efficiently assisted in the operation and maintenance of the Van de Graaff.

---

†Work performed in part under the auspices of the National Science Foundation and the U. S. Atomic Energy Commission.

*Now at the University of Liverpool, Liverpool, England.

[1]S. Cohen and D. Kurath, Nucl. Phys. 73, 1 (1965).

[2]J. B. Thomas, P. Paul, S. S. Hanna, D. C. Camp, and G. A. Armantrout, Bull. Am. Phys. Soc. 11, 26 (1966).

[3]K. G. Kibler, Phys. Rev. 152, 932 (1966).

[4]J. B. Marion, Nucl. Data A4, 301 (1966).

[5]A. E. Blaugrund, D. H. Youngblood, G. C. Morrison, and R. E. Segel, Phys. Rev. 158, 893 (1967).

[6]Supplied by Stable Isotopes Division, Oak Ridge National Laboratory, Oak Ridge, Tennessee.

[7]E. K. Warburton, J. W. Olness, and A. R. Poletti, Phys. Rev. 155, 1164 (1967). A Doppler shift of 0.9 ± 0.6 keV was added to their reported $E_\gamma = 1020.4 \pm 1.0$ keV for the 2.10 → 1.08-MeV transition in F^{18}.

[8]C. F. Williamson, J.-P. Boujot, and J. Picard, Centre D'Etudes Nucleaires de Saclay Report No. CEA-R 3042, 1966 (unpublished).

[9]W. Whaling, in *Handbuch der Physik*, edited by S. Flügge (Springer-Verlag, Berlin, Germany, 1958), Vol. 34, p. 193; S. K. Allison, D. Auton, and R. A. Morrison, Phys. Rev. 138, A688 (1965); S. A. Teplova, I. S. Dimitriev, V. S. Nikolaev, and L. N. Fateeva, Zh. Eksperim. i Teor. Fiz. 32, 974 (1957) [transl.: Soviet Phys. – JETP 5, 797 (1957)].

[10]J. F. Janni, Air Force Weapons Laboratory Report No. AFWL-TR-65-150, 1966 (unpublished).
[11]S. W. Robinson and R. D. Bent, Phys. Rev. 168, 1266 (1968).
[12]L. F. Chase, Jr., R. G. Johnson, F. J. Vaughn, and E. K. Warburton, Phys. Rev. 127, 859 (1962).
[13]Chromium Corporation of America, Grade C (light tight, with a thickness variation of ±20%).
[14]M. J. Throop, G. C. Morrison, and D. H. Youngblood, Bull. Am. Phys. Soc. 13, 606 (1968).
[15]D. Kurath, private communication.
[16]E. K. Warburton, J. W. Olness, S. D. Bloom, and A. R. Poletti, Phys. Rev. 171, 1178 (1968).
[17]F. C. Barker, private communication quoted in Ref. 2.

PHYSICAL REVIEW C VOLUME 3, NUMBER 2 FEBRUARY 1971

Survey of (p, t) Reactions in the $1p$ Shell*

S. Kahana
Brookhaven National Laboratory, Upton, New York 11973
and
D. Kurath†
State University of New York, Stony Brook, New York 11790
(Received 5 November 1970)

A comprehensive survey of 21 (p,t) reactions for a wide range of $1p$-shell nuclei is made using zero-range distorted-wave Born-approximation codes and previously calculated two-particle fractional parentage coefficients. Average optical parameters are used for the proton and triton potentials in an attempt to relate magnitudes of transitions in different nuclei. A reasonable fit is obtained to the experimental data, but there remain discrepancies in strong transitions for target nuclei with $A \geq 14$. An effect of $(2s\text{-}1d)$ admixture which acts differently in $L=0$ and $L=2$ transfer is proposed as a likely explanation of this difficulty.

I. INTRODUCTION

In principle, the two-nucleon-transfer reaction is a sensitive probe of nuclear structure. In practice it is also a sensitive probe of the nuclear-reaction theory. Most properties of the nuclei between He^4 and O^{16} are well described in terms of $1p$ configurations for the nuclear wave functions. A study[1] of the (d, p) reaction in this region has shown that the extracted spectroscopic information is in good agreement with calculated $1p$ values if average parameters are used in the optical-model calculations. It seemed worthwhile to us to perform a survey of the two-particle transitions in the same spirit. Cohen and Kurath[2] have published the structural ingredients of such a survey, the two-particle fractional parentage coefficients (c.f.p.'s).

A large number of two-particle-transfer reactions have been measured in the $1p$ region. Most experiments have been interpreted using some form of distorted-wave Born-approximation (DWBA) analysis. However, differential optical potentials are used in the analyses, and often only the shape of the angular distribution (and hence the transferred L value) is determined. Certainly no attempt has been made to relate magnitudes of cross sections for states in different nuclei. The possibility least fraught with complication is presented by 20 (p, t) transitions with incident proton energy between 40 and 50 MeV and target mass number A between 10 and 16. In analyzing these transitions we have made extensive use of the zero-range DWBA codes TWO PAR and DWUCK, and are grateful to their respective authors, B. F. Bayman and P. D. Kunz, for their kind cooperation.

Our first concern is to see how well one can represent the observed angular distributions and magnitudes of the cross sections with an average optical potential containing a single normalization parameter. Secondly, there is the possibility of investigating the spectra of isobaric analog states for which structure calculations often give large amplitudes and distinctive state-dependent variation. Finally, should first-order agreement with experiment be obtained, it may prove possible to look for small admixtures of $(2s\text{-}1d)$ components in the nuclear wave functions.

Section II is devoted to a comparison of experiment with calculations based on the $1p$ shell model and to some comments on the results of this comparison. Section III contains a discussion divided between a brief consideration of the validity of the DWBA analysis and a calculation of the effects of $(2s\text{-}1d)$ admixtures.